Frequency comb generation in a silicon ring resonator modulator

IOSIF DEMIRTZIOGLOU,* COSIMO LACAVA, KYLE R. H. BOTTRILL, DAVID J. THOMSON, GRAHAM T. REED, DAVID J. RICHARDSON, AND PERIKLIS PETROPOULOS

Optoelectronics Research Centre, University of Southampton, Southampton SO17 1BJ, UK
**I.Demirtzioglou@soton.ac.uk*

Abstract: We report on the generation of an optical comb of highly uniform in power frequency lines (variation less than 0.7 dB) using a silicon ring resonator modulator. A characterization involving the measurement of the complex transfer function of the ring is presented and five frequency tones with a 10-GHz spacing are produced using a dual-frequency electrical input at 10 and 20 GHz. A comb shape comparison is conducted for different modulator bias voltages, indicating optimum operation at a small forward-bias voltage. A time-domain measurement confirmed that the comb signal was highly coherent, forming 20.3-ps-long pulses.

© 2017 Optical Society of America under the terms of the OSA Open Access Publishing Agreement

OCIS codes: (130.3120) Integrated optics devices; (230.5750) Resonators.

References and links

1. P. De Dobbelaere, G. Armijo, J. Balardeta, B. Chase, Y. Chi, A. Dahl, Y. De Koninck, S. Denton, M. Eker, S. Fathpour, D. Foltz, F. Gholami, S. Gloeckner, K. Y. Hon, S. Hovey, S. Jackson, W. Li, Y. Liang, M. Mack, G. Masini, G. McGee, A. Mekis, S. Pang, M. Peterson, T. Pinguet, L. Planchon, K. Roberson, S. Sahni, J. Schramm, M. Sharp, C. Sohn, K. Stechschulte, P. Sun, G. Vastola, S. Wang, B. Weber, G. Wong, K. Yokoyama, S. Yu, and R. Zhou, "Silicon-photonics-based optical transceivers for high-speed interconnect applications," Proc. SPIE **9775**, 977503 (2016).
2. A. Martin, J. Luff, D. Feng, and M. Asghari, "Technical Challenges for 100Gb / s Silicon Photonics Transceivers for Data Center Applications," in *Opt. Fiber Commun. Conf. 2016* (2016), pp. 1–3.
3. L. Chen, C. Doerr, R. Aroca, S. Y. Park, J. C. Geyer, T. Nielsen, C. Rasmussen, and B. Mikkelsen, "Silicon Photonics for 100G-and-beyond Coherent Transmissions," *Opt. Fiber Commun. Conf.* (2016), paper Th1B.1.
4. F. Boeuf, S. Cremer, E. Temporiti, M. Fere, M. Shaw, N. Vulliet, B. Orlando, D. Ristoiu, A. Farcy, A. Mekis, G. Masini, P. Sun, Y. Chi, H. Petiton, S. Jan, J.-R. Manouvrier, C. Baudot, P. Le Maitre, J.-F. Carpentier, L. Salager, M. Traldi, L. Maggi, D. Rigamonti, C. Zaccherini, and C. Elemi, "Recent Progress in Silicon Photonics R & D and Manufacturing on 300mm Wafer Platform," in *Opt. Fiber Commun. Conf.* (2015), pp. 4–6.
5. A. Moscoso-Mártir, J. Müller, J. Hauck, N. Chimot, R. Setter, A. Badihi, D. E. Rasmussen, A. Garreau, M. Nielsen, E. Islamova, S. Romero-García, B. Shen, A. Sandomirsky, S. Rockman, C. Li, S. S. Azadeh, G.-Q. Lo, E. Mentovich, F. Merget, F. Lelarge, and J. Witzens, "Silicon photonics WDM transceiver with SOA and semiconductor mode-locked laser," Opt. Express **25**(1), 1395–1401 (2016).
6. G. Li, D. Lambert, J. Zyskind, J. Spann, M. Askari, G. Pickrell, M. Sodagar, and S. Krasulick, "100Gb/s CWDM transmitter and receiver chips on a monolithic Si-photonics platform," in *IEEE Int. Conf. Gr. IV Photonics GFP* (2016), pp. 164–165.
7. H. Füser, A. L. Giesecke, A. Prinzen, S. Suckow, C. Porschatis, H. Lerch, M. M. Tarar, J. Bolten, T. Wahlbrink, and H. Kurz, "56 Gb/s WDM transmitter module based on silicon microrings using comb lasers," in *CLEO Si* (2015), pp. 2–3.
8. J. Pfeifle, V. Brasch, M. Lauermann, Y. Yu, D. Wegner, T. Herr, K. Hartinger, P. Schindler, J. Li, D. Hillerkuss, R. Schmogrow, C. Weimann, R. Holzwarth, W. Freude, J. Leuthold, T. J. Kippenberg, and C. Koos, "Coherent terabit communications with microresonator Kerr frequency combs," Nat. Photonics **8**(5), 375–380 (2014).
9. P. Del'Haye, T. Herr, E. Gavartin, R. Holzwarth, and T. J. Kippenberg, "Octave spanning frequency comb on a chip," Opt. Express **19**(15), 1–6 (2009).
10. Y. Okawachi, K. Saha, J. S. Levy, Y. H. Wen, M. Lipson, and A. L. Gaeta, "Octave-spanning frequency comb generation in a silicon nitride chip," Opt. Lett. **36**(17), 3398–3400 (2011).
11. A. M. Kaplan, A. Greenblatt, G. Harston, P. S. Cho, Y. Achiam, and I. Shpantzer, "Tunable Frequency Comb Generator based on LiNbO3 Ring Resonator," Coherent Opt. Technol. Appl. **3**, 3–5 (2006).
12. M. Yamamoto, Y. Tanaka, T. Shioda, T. Kurokawa, and K. Higuma, "Optical frequency comb generation using dual frequency optical phase modulation," in *Integrated Photonics Research and Applications*, Optical Society of America (2005), paper ITuF5.

13. N. Dupuis, C. R. Doerr, L. Zhang, L. Chen, N. J. Sauer, P. Dong, L. L. Buhl, and D. Ahn, "InP-based comb generator for optical OFDM," J. Lightwave Technol. **30**(4), 466–472 (2012).
14. R. Slavík, S. G. Farwell, M. J. Wale, and D. J. Richardson, "Compact Optical Comb Generator Using InP Tunable Laser and Push – Pull Modulator," IEEE Photonics Technol. Lett. **27**(2), 217–220 (2015).
15. R. Wu, V. R. Supradeepa, C. M. Long, D. E. Leaird, and A. M. Weiner, "Generation of very flat optical frequency combs from continuous-wave lasers using cascaded intensity and phase modulators driven by tailored radio frequency waveforms," Opt. Lett. **35**(19), 3234–3236 (2010).
16. S. Ozharar, F. Quinlan, I. Ozdur, S. Gee, and P. J. Delfyett, "Ultraflat optical comb generation by phase-only modulation of continuous-wave light," IEEE Photonics Technol. Lett. **20**(1), 36–38 (2008).
17. T. Sakamoto, T. Kawanishi, and M. Izutsu, "Asymptotic formalism for ultraflat optical frequency comb generation using a Mach-Zehnder modulator," Opt. Lett. **32**(11), 1515–1517 (2007).
18. T. Sakamoto, T. Kawanishi, and M. Izutsu, "Widely wavelength-tunable ultra-flat frequency comb generation using conventional dual-drive Mach-Zehnder modulator," Electron. Lett. **43**(19), 1039–1040 (2007).
19. C. Weimann, P. C. Schindler, R. Palmer, S. Wolf, D. Bekele, D. Korn, J. Pfeifle, S. Koeber, R. Schmogrow, L. Alloatti, D. Elder, H. Yu, W. Bogaerts, L. R. Dalton, W. Freude, J. Leuthold, and C. Koos, "Silicon-organic hybrid (SOH) frequency comb sources for terabit/s data transmission," Opt. Express **22**(3), 3629–3637 (2014).
20. J. E. Heebner, A. Vincent Wong, A. Schweinsberg, R. W. Boyd, and D. J. Jackson, "Optical transmission characteristics of fiber ring resonators," IEEE J. Quantum Electron. **40**(6), 726–730 (2004).
21. R. A. Soref and B. R. Bennett, "Electrooptical effects in silicon," IEEE J. Quantum Electron. **23**(1), 123–129 (1987).
22. K. R. H. Bottrill, G. D. Hesketh, F. Parmigiani, P. Horak, D. J. Richardson, and P. Petropoulos, "Suppression of gain variation in a PSA-based phase regenerator using an additional harmonic," IEEE Photonics Technol. Lett. **26**(20), 2074–2077 (2014).
23. K. Bottrill, M. A. Ettabib, J. C. Gates, C. Lacava, F. Parmigiani, D. J. Richardson, and P. Petropoulos, "Flexible scheme for measuring chromatic dispersion based on interference of frequency tones," in *Opt. Fiber Commun. Conf.* (2017), paper Th4H.5.

1. Introduction

Silicon photonics has rapidly become one of the most popular candidates for the implementation of high-speed, short-reach interconnects in data-center and computer networks, and a number of transceiver systems adopting the technology have already become a commercial reality [1–4]. In order to increase the data-rate per transceiver-unit, the adoption of Wavelength-Division Multiplexing (WDM) is currently being considered [5–7]. These WDM carriers are usually generated using integrated Distributed Feedback (DFB) laser arrays, in which each DFB operates separately from one another. However, the concept of frequency comb generation has also been employed as an alternative to the use of multiple lasers on a single chip. Previous demonstrations have used micro-ring resonators on both silicon nitride- and silica-based designs for the generation of broadband combs, benefitting from the nonlinear properties of the materials [8–10]. The line spacing of these types of combs is dependent on the free spectral range (FSR) of the cavity and can reach tens or hundreds of GHz. However, the main limitation associated with this technique is the requirement for optical pump power levels in the order of Watts or hundreds of mW, with no means of control over the distribution of this power to the generated lines.

Alternatively, a frequency comb can be generated through electro-optic modulation, using a radio frequency (RF) wave as the driving signal. Then the number of the generated comb lines is dependent on the achievable modulation depth and their spacing is solely determined by the frequency of the RF signal. Most implementations employ phase modulation, since it is more efficient in generating high-order harmonics. Demonstrations of this technique have been presented on $LiNbO_3$ modulators [11, 12], as well as InP-based integrated devices [13, 14], while significant efforts have also been made towards improving the flatness of these combs, mainly by appropriately tailoring the electrical input [12, 15–18]. The most notable application of this work on a silicon platform made the use of a silicon-organic-hybrid (SOH) Mach-Zehnder Modulator (MZM) and demonstrated the generation and transmission of WDM signals [19].

In this work, we use a micrometer-scale ring resonator modulator (RRM) fabricated on the silicon-on-insulator (SOI) platform for the generation of highly uniform comb lines as required in WDM applications. An RRM has been chosen for this purpose, because of its

small footprint and large modulation depth, whereas electro-optic modulation allows flexibility in the choice of line spacing. We present an experimental characterization of the complex transfer function of the RRM and study the effects of the coupling condition and the modulation regime on the comb shape. The coherence of the output is verified through temporal measurements of the comb waveform. This is to our knowledge, the first investigation of the potential of a small-footprint, low-power silicon modulator for frequency comb generation on a chip, and can form the basis for low-cost comb generation based on CMOS-compatible fabrication processes.

2. Experimental setup and ring design

The frequency comb generation is based on electro-optic modulation of a CW source in a silicon RRM, resulting in the production of a number of sidebands that can function as individual optical carriers. The factors that determine the properties of the generated comb are the electrical driving signal waveform and the achieved modulation depth. In the case of a silicon RRM, the latter is defined by the coupling condition of the ring and the operating regime of the p-n junction. For this reason, sections 2 and 3 present the physical properties of the ring, along with a characterization of its complex transfer function.

The most important parameters in the design of the RRM are the ring diameter and the bus-ring separation gap. They determine the round-trip loss and the bus-ring power coupling ratio, which in turn determine the coupling regime [20]. The three different coupling regimes of a ring resonator are illustrated in Fig. 1, in transfer function graphs for the intensity and phase. For a given value of the round-trip loss, there is a distance d_{crit} between the bus and the ring, for which the transmission at the resonance wavelengths is zero and the phase exhibits an abrupt π-radian shift (critical coupling). When the bus-ring distance is shorter (longer) than d_{crit}, the ring is overcoupled (undercoupled). In both overcoupling and undercoupling, the intensity trough is not as deep as in the critical coupling point, while the phase experiences a π-radian delay at the resonance wavelengths in the former case and a wiggle in the latter. The RRM in this work had a 24-μm diameter with a bus-ring gap d equal to 240 nm and was measured to be slightly off the critical coupling point, inside the overcoupling regime for no applied voltage.

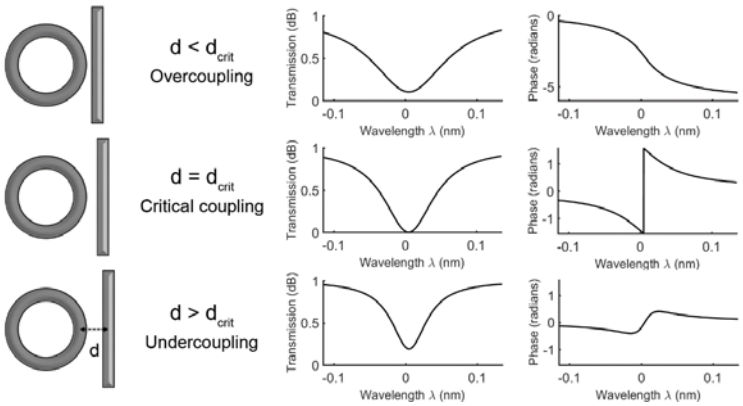

Fig. 1. Coupling regimes and respective theoretical transfer functions of a ring resonator around the resonance wavelength.

The structure was fabricated on the SOI platform with CMOS-compatible processes. Deep Ultraviolet (DUV) lithography was employed to write the silicon photonic circuit pattern and phosphorus and boron implantation was used to dope the ring circumference with carriers, forming the p-n junction structure. A top-view micrograph of the ring is illustrated in Fig. 2, along with a schematic representation of the cross-section of the doped parts of the waveguide. Coupling to the device was enabled by a set of grating couplers, as depicted in the

micrograph, which were designed to guide only the TE mode within the C-band (mode principal axis in the x-direction in Fig. 2(b)). Two PM fibers were mounted at an angle of 11° relative to the surface normal of the chip and aligned to the grating couplers in order to launch and collect light (see Fig. 2(c)).

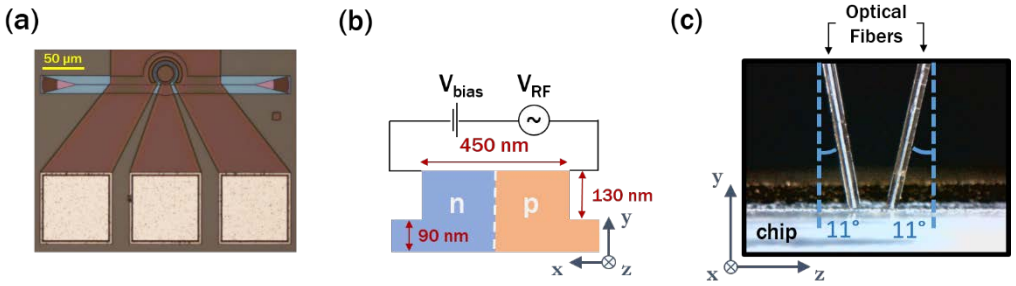

Fig. 2. (a) Ring resonator modulator top view micrograph, (b) waveguide cross-section and (c) coupling scheme for the silicon photonic chip.

Application of voltage to the p-n junction of the doped waveguide was facilitated by a three-pin high-speed probe which contacted a set of metallic pads connected to the p-n junction of the device (Fig. 2(a)). Electrical biasing of the p-n junction induced a change in the properties of the guided mode, as determined by the expressions derived by Soref and Bennett, quantifying the effect of carrier density change to the refractive index and absorption of silicon [21]. Therefore, changes in the depletion area of the junction as well as carrier injection altered the doped waveguide mode, and this effect is described by the change experienced by the complex effective refractive index:

$$\Delta\tilde{n}_{eff} = \Delta n_{eff} + i\Delta a \qquad (1)$$

where Δn_{eff} is the change in the effective refractive index and $\Delta\alpha$ is the change in the absorption. The electro-refractive and electro-absorptive effects caused by the bias voltage modify the RRM transfer function in two aspects: Δn_{eff} causes a wavelength shift and $\Delta\alpha$ affects the resonance shape and depth, because changes in the round-trip loss alter the coupling condition. To analyze this effect, we conducted characterization measurements of the complex transfer function of the device.

3. Device characterization

The intensity transfer function of the device was measured using a tunable laser. A wavelength sweep of a 1-pm step revealed the spectral profile depicted in Fig. 3(a) for different DC voltages applied to the p-n junction. The shape and depth of the resonances indicate that critical coupling occurs at a forward bias voltage of 1 V, while lower (including reverse bias) and higher voltages correspond to an overcoupling and an undercoupling state, respectively. Also, stronger effects are apparent in forward bias compared to reverse bias. This is because a small forward-bias voltage narrows the p-n junction depletion region, leading to a larger overlap with the optical mode, while even higher voltages (> + 0.7 V) induce carrier injection which greatly affects the effective refractive index and absorption of the mode but is a slower physical phenomenon. Therefore, although critical coupling is desired in our device to maximize the achieved modulation depth, operating inside the carrier injection regime hinders modulation at frequencies higher than ~1 GHz. This tradeoff is shown in the generated comb shapes in the following section. It is also noted that the Q-factors extracted from the transfer functions are in the range of 3,000 to 10,000, corresponding to photon cavity lifetimes smaller than 8 ps, therefore the resonator geometry is not the limiting factor in terms of bandwidth in this device.

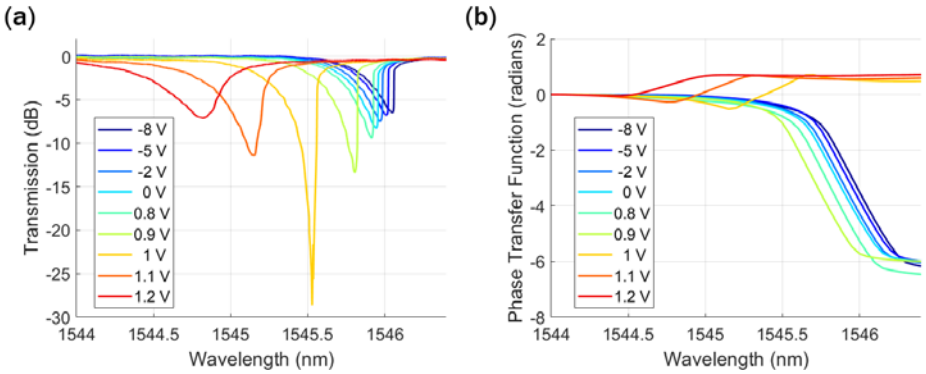

Fig. 3. Measured (a) intensity and (b) phase transfer function (resolution: 50 pm) of the ring resonator modulator and their change vs. applied bias voltage.

The RRM's phase transfer function was also measured and is illustrated in Fig. 3(b) for different DC bias voltages. In order to measure the phase profile of our device we constructed a purpose-built measurement system to extract the illustrated graph. The measurement involves launching two closely spaced coherent spectral tones into the device and through heterodyne detection, measuring the phase difference they acquire after propagation. The mathematical formulation and experimental implementation of this method are thoroughly described in [22] and [23]. The phase profile of the device near the resonance wavelengths reveals the expected phase jumps that were previously described. Therefore, strong phase modulation can be achieved on the RRM by operating it close to the resonance. In the generation of a flat comb shape, this phase modulation is key to reducing the power level of the fundamental tone, because the strength of the carrier can be diminished in the spectrum since its phase inverses its sign throughout the voltage swing. Depending on the spectral position of the tone relative to the resonance point, it experiences different levels of suppression, thus providing a means of tuning its power level to equalize the comb lines.

4. Results and discussion

The frequency comb generation was implemented experimentally using the setup of Fig. 4. The RRM was driven by two electrical tones at 10 and 20 GHz, which were produced by two RF clocks and subsequently amplified and sent to the metallic pads of the photonic chip via a high-speed probe. A phase shifter allowed tuning of the phase difference between the two RF signals, and a bias tee was used to set the bias voltage of the p-n junction. The two RF frequencies were selected in order to produce at least five frequency tones at a 10-GHz spacing. Testing with input frequencies higher than 20 GHz did not result in sufficiently strong spectral tones for a flat shape, limited by the bandwidth of the RRM.

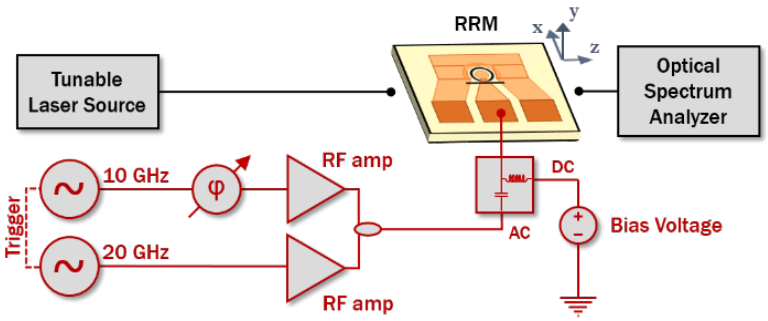

Fig. 4. Experimental setup for the frequency comb generation. Lines in black represent optical connections, while lines in red represent electrical connections.

This set-up allowed enough flexibility to enable fine-tuning of the spectral output of the RRM with regard to flatness and overall power level. We used an optical input power of 2.3 dBm to the RRM throughout all experiments in order to produce sufficiently strong comb lines relative to the noise floor. In this respect, we were limited by the detrimental effect that higher optical power levels would cause to the modulation depth of the device due to onset of nonlinear effective refractive index changes and nonlinear losses inside the ring. We generated a frequency comb consisting of five spectral tones with a 0.7 dB maximum power difference among them, at a spacing of 10 GHz (Fig. 5(a)). This was obtained with an electrical input comprising a 1.5-V_{pp} 10-GHz tone and a 2.9-V_{pp} 20-GHz tone whose phase difference was π radians, and a bias voltage of + 0.22 V. It is noted that the amplitudes of our RF signals were limited by the gain of the RF amplifiers used. The on-chip insertion loss of the device amounted to 5.5 dB.

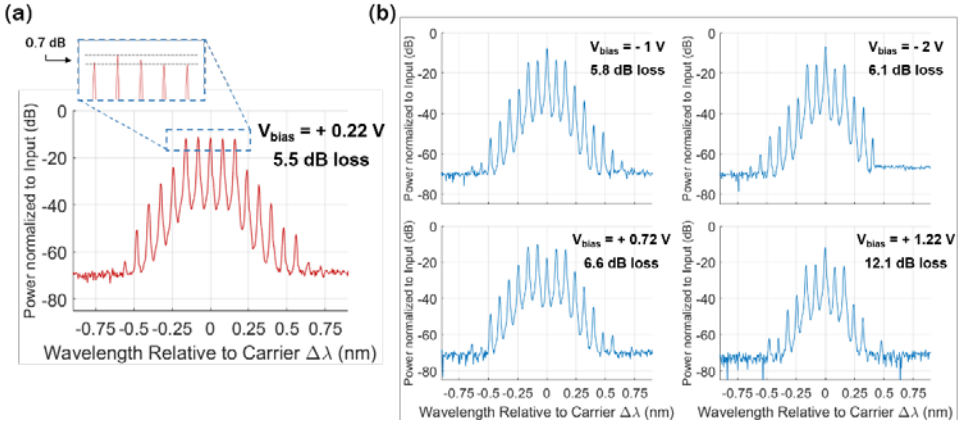

Fig. 5. (a) Generated frequency comb at 10 GHz line spacing for a 0.22-Volt forward bias voltage applied, (b) Generated frequency combs for different bias voltages applied. Top and bottom rows correspond to reverse and forward bias respectively.

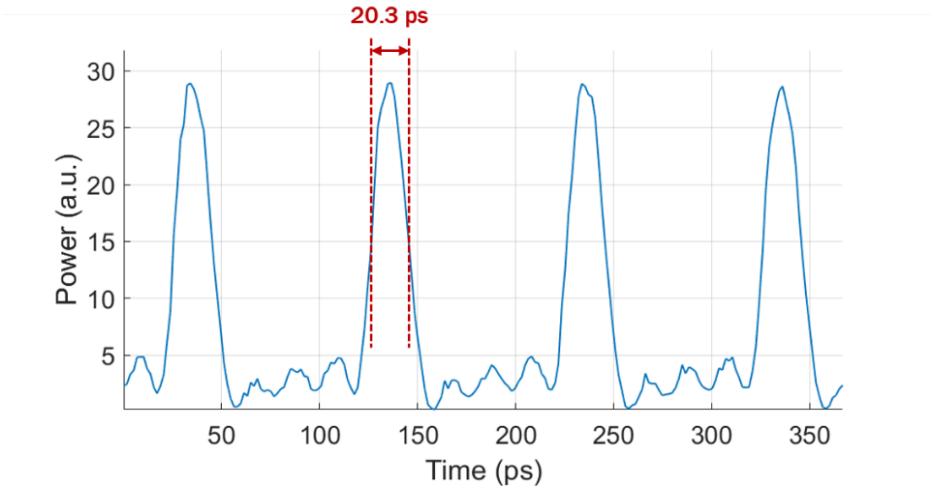

Fig. 6. Measured optical pulses generated at the output of the device, by means of an optical sampling oscilloscope.

As described in the previous section, the key factors in generating a flat comb shape are the intensity and phase modulation depths. Both of them affect the power level of the sidebands but phase modulation also enables manipulation of the carrier power level. The

operating condition of the comb was optimized by monitoring the variation of the comb shape while tuning the bias voltage of the modulator and the wavelength of the CW source. Figure 5(b) portrays different comb shapes collected at various bias voltage values, spanning both reverse- and forward-bias regimes. The input wavelength was tuned in every case to produce the best possible outcome in terms of comb flatness. In the reverse-bias case, the modulation depth was not adequate to produce a flat comb shape, owing to the relatively low resonance depth (Fig. 3(a)). In the forward-bias case, the tradeoff discussed in the previous section is apparent: moving towards critical coupling also moves the p-n junction towards carrier injection which hinders the generation of high-frequency sidebands. Operating voltages higher than ~0.7 V caused a drop in the power level of the comb lines. Therefore, a bias voltage of + 0.22 V proved to be the optimum point of operation.

A time-domain measurement of the device output was conducted next, to verify the coherence of the comb lines. Pulses of a full-width at half-maximum (FWHM) of 20.3 ps were recorded (Fig. 6) using an optical sampling oscilloscope (EXFO PSO-102). The period of the pulses corresponded to the 10-GHz line spacing, thus yielding a duty cycle of 20%, which indicates close to transform-limited pulses for the spectrum we recorded.

The comb generation technique proposed in this paper enjoys the benefits of a small footprint and a low overall power consumption. The area occupied by the RRM and the electrical pads is 0.062 mm^2, which offers increased compactness compared to MZM implementations, such as the mm-sized structure in [19]. Moreover, at the cost of electronic complexity (i.e. the use of two RF tones), the system uses a conventional integrated component to tune the shape of the generated comb with an electrical power consumption in the range of tens of milliWatts. However, the bandwidth of the modulator used here has limited the achievable comb spacing to ~10 GHz and the number of lines is dependent on the external RF excitation. Reduction in power consumption and further broadening of the comb span can be achieved by optimizing the ring design for critical coupling far from the carrier-injection regime, as well as through the adoption of cascaded ring designs.

5. Conclusion

We have demonstrated the generation of a coherent optical frequency comb in the C-band, comprising five 10-GHz-spaced spectral lines, by means of electro-optic modulation of a low-power optical carrier in a ring resonator fabricated on the SOI platform. Appropriate tuning of the electrical input offered the possibility to tailor the comb shape, limiting the maximum power variation between the lines to 0.7 dB. Operating near the critical coupling point while remaining adequately far from the carrier injection regime of the p-n junction proved to be the optimum point of operation. The comb lines were also proven to be mutually coherent, resulting in the generation of transform-limited pulses. This work demonstrates the potential for flexible generation of multiple optical carriers on an integrated transceiver using conventional silicon modulators.

Acknowledgments

This work has been supported by the Engineering and Physical Sciences Research Council (EPSRC), UK through the Silicon Photonics for Future Systems (SPFS) Programme Grant (EP/L00044X/1) and the Converged Optical and Wireless Access Networks (COALESCE) Programme Grant (EP/P003990/1). D. J. Thomson acknowledges funding from the Royal Society for his University Research Fellowship. The data for this work is accessible through the University of Southampton Institutional Research Repository: https://doi.org/10.5258/SOTON/D0277.